Journal of Computational Physics 227 (2008) 9389–9407

Contents lists available at ScienceDirect

Journal of Computational Physics

journal homepage: www.elsevier.com/locate/jcp

A gas-kinetic BGK scheme for semiclassical Boltzmann hydrodynamic transport

Yu-Hsin Shi, J.Y. Yang *

Institute of Applied Mechanics, National Taiwan University, Taipei 10764, Taiwan

ARTICLE INFO

Article history:
Received 19 January 2008
Received in revised form 17 June 2008
Accepted 19 June 2008
Available online 18 July 2008

Keywords:
Quantum hydrodynamics
Gas-kinetic scheme
Quantum gas
Semiclassical Boltzmann equation
Quantum Navier–Stokes solution

ABSTRACT

A class of gas-kinetic BGK schemes for solving quantum hydrodynamic transport based on the semiclassical Boltzmann equation with the relaxation time approximation is presented. The derivation is a generalization to the development of Xu [K. Xu, A gas-kinetic BGK scheme for the Navier–Stokes equations and its connection with artificial dissipation and Godunov method, from gas-kinetic theory, J. Comput. Phys. 171 (2001) 289–335] for the classical gas. Both Bose–Einstein and Fermi–Dirac gases are considered. Some new features due to the quantum equilibrium distributions are delineated. The first-order Chapman–Enskog expansion of the quantum BGK-Boltzmann equation is derived. The coefficients of shear viscosity and thermal conductivity of a quantum gas are given. *The van Leer's limiter is used to interpolate and construct the distribution on interface to achieve second-order accuracy*. The present quantum gas-kinetic BGK scheme recovers the Xu's scheme when the classical limit is taken. Several one-dimensional quantum gas flows in a shock tube are computed to illustrate the present method.

1. Introduction

It is well known that the classical hydrodynamic transport (or conservation) equations can be derived from physical arguments or from a moment expansion of the Boltzmann equation. The class of equations covered includes the solution of respectively, the Euler, Navier–Stokes, Burnett and super-Burnett equations depending on the order of the Chapman–Enskog expansion of the Boltzmann equation. Computationally, the direct simulation Monte Carlo (DSMC) method is the most well known method for solving the Boltzmann equation and has been widely used in simulating rarefied gas dynamical flows, see [3]. To avoid the complex collision integral term of the Boltzmann equation, a simple and physical model, the relaxation time approximation, was proposed by Bhatnagar, Gross and Krook (BGK) [2], which rendered the final governing equation a nonlinear inhomogeneous differential equation. This allows either direct integration of the differential equation or deterministic numerical solution in phase space possible. A deterministic high resolution scheme based on discrete ordinate method for solving BGK Boltzmann equation has been presented by Yang and Huang [25]. In recent years, the gas-kinetic schemes constructed based on the solution of the BGK-Boltzmann equation by Xu [21–24] have been applied and extended to many classical hydrodynamic flows with great success. Also, a so-called railroad method for the construction of kinetic schemes up to the full-Burnett equations has been presented by Ohwada [17]. The consistency between the traditional Chapman–Enskog expansion and the successive approximation for the BGK equation up to the super-Burnett order has been illustrated.

Analogous to the classical Boltzmann equation, a semiclassical Boltzmann equation for transport phenomenon can be developed for fermions and bosons, see [19,14]. The Chapman–Enskog procedure has been generalized for quantum gases

* Corresponding author. Tel.: +886 2 3366 5636; fax: +886 2 2362 9290.
E-mail address: yangjy@iam.ntu.edu.tw (J.Y. Yang).

0021-9991/$ - see front matter © 2008 Elsevier Inc. All rights reserved.
doi:10.1016/j.jcp.2008.06.036

to obtain the expressions for the transport coefficients such as shear viscosity and thermal conductivity. More recent works on the derivation of hydrodynamic equations of a trapped dilute Bose gas based on quantum Boltzmann equation using Chapman–Enskog procedure have been given by Nikuni and Griffin [16]. The quantum conservation laws have the same form as their classical counterparts. However, to close the moment expansion at the three moments for hydrodynamics, one must define the other higher moments in terms of the particle number density, momentum density and energy density. A DSMC method for treating the Uehling and Uhlenbeck Boltzmann equation has been given by Garcia and Wagner [8]. The quantum correction to the energy density was first derived by Wigner [20]. The behavior of a quantum fluid near thermal equilibrium and in the high temperature limit can be approximated by adding $O(h^2)$ corrections to the classical fluid dynamical equations. The $O(h^2)$ terms allow particle tunnelling through potential barriers and particle buildup in potential wells, see [9,10]. An interesting study on the rarefied classical and quantum gas flows based on kinetic Boltzmann equation has been given by Beyer [1].

The concept of relaxation time approximation proposed by Bhatnagar, Gross, and Krook provides a very physical and useful simplification of the complicated collision integral of the Boltzmann equation and makes the direct solution of the BGK-Boltzmann equation more tractable. And indeed, many extension and generalization of this concept to other carriers transport such as electron and phonon transport in semiconductors have been commonly used, see [15]. Also, the BGK-Boltzmann type governing equations are widely used in micro- and nano-scale energy transports, see [5].

Beyond the kinetic schemes for the zeroth-order solution of the Boltzmann equations (i.e., Euler solution), there are several kinetic numerical methods for higher-order extensions to Navier–Stokes equations have been developed, for examples, [21,6,17]. In particular, the main feature of the gas-kinetic BGK schemes developed by Xu [23] is that the effect of particle collisions has been taken into account in the gas evolution stage or flux evaluation process at a cell interface within a time step, from which a time-dependent gas distribution function and the resulting numerical fluxes at the cell interface can be obtained. Due to the intrinsic connection between the BGK model and the viscous governing equations, the gas-kinetic BGK method gives Navier–Stokes solutions directly in smooth regions. In the discontinuous regions, the scheme provides a delicate dissipative mechanism to yield a stable and crisp shock transition, and the scheme becomes a shock-capturing method. Since the gas revolution process in the BGK method is a relaxation from non-equilibrium state to an equilibrium one, the entropy condition is always satisfied in the BGK method, see [23].

In this work, we shall adopt the relaxation time approximation to replace the collision integral of the Uehling–Uhlenbeck Boltzmann equation for a rarefied quantum gas and develop a class of gas-kinetic BGK scheme for quantum hydrodynamic transport which is parallel to the classical counterpart of Xu. The main difference between the classical and quantum development is due to the more complex form of the quantum equilibrium distribution function i.e., Bose–Einstein or Fermi–Dirac distribution, as compared to the classical one, i.e., Maxwell–Boltzmann distribution function. Various orders of moments of both quantum equilibrium distribution function and its first-order derivative needed in the construction of the present quantum BGK scheme are systematically derived (given in the Appendix).

The paper is organized as following. In Section 2, we first briefly describe the elements of Uehling–Uhlenbeck Boltzmann transport equation. Its connection to hydrodynamic equations is outlined. The quantum BGK model is adopted and the zeroth and first-order solutions of Chapman–Enskog procedure are described. In Section 3, the main framework of quantum gas-kinetic BGK scheme is described in detail. The quantum Navier–Stokes order distribution function at cell interface is derived. The moments of both quantum equilibrium distribution function and its first-order derivative are defined. In Section 4, the role of relaxation time played in quantum BGK and its determination are discussed. In Section 5, some numerical experiments using one-dimensional quantum gas flow in a shock tube are given to illustrate the present method. Finally, some concluding remarks are given in Section 6. Formulation of some half-ranged moments of the quantum equilibrium distribution function is included in the Appendix.

2. Elements of quantum Boltzmann equation

In this section, we briefly describe the elements of quantum Boltzmann transport equation relevant to the development of present work. Following [14], we consider the extension of the Boltzmann equation to quantum systems due to Uehling and Uhlenbeck [19] which they took the Pauli exclusion principle into account,

$$\left(\frac{\partial}{\partial t}+\frac{\vec{p}}{m}\cdot\nabla_{\vec{x}}-\nabla V(\vec{x},t)\cdot\nabla_{\vec{p}}\right)f(\vec{p},\vec{x},t)=\left(\frac{\delta f}{\delta t}\right)_{\text{coll.}}^{\text{UU}}, \tag{1}$$

where m is the particle mass, V is the mean field potential and $f(\vec{p},\vec{x},t)$ is the distribution function which represents the average density of particles with momentum $\vec{p}$ at the space–time point $\vec{x},t$. The $(\delta f/\delta t)_{\text{coll.}}^{\text{UU}}$ denotes the collision term according to Uehling and Uhlenbeck, it takes the form,

$$\left(\frac{\delta f}{\delta t}\right)_{\text{coll.}}^{\text{UU}}=\int \mathrm{d}\vec{p}\int \mathrm{d}\Omega K(\vec{p},\vec{q},\Omega)\{[1+\theta f(\vec{p},t)][1+\theta f(\vec{q})]f(\vec{p}^*,t)f(\vec{q}^*,t)-[1+\theta f(\vec{p}^*,t)][1+\theta f(\vec{q}^*)]f(\vec{p},t)f(\vec{q},t)\}, \tag{2}$$

where the function K is the collision kernel, Ω is the solid angle and $\theta=+1$ denotes the case of Bose–Einstein statistics and $\theta=-1$ denotes the case of Fermi–Dirac statistics. It is noted that the Boltzmann equation of the classical statistics is included in Eq. (2) as a special case when $\theta=0$. To avoid the complexity of the collision integral in different type of collision, the

relaxation time model originally proposed by Bhatnagar, Gross and Krook (BGK) [2] for the classical non-relativistic neutral and charged gases has been widely used. The model Boltzmann equation in the quantum case can be expressed as

$$\left(\frac{\partial}{\partial t}+\frac{\vec{p}}{m}\cdot\nabla_{\vec{x}}-\nabla V(\vec{x},t)\cdot\nabla_{\vec{p}}\right)f(\vec{p},\vec{x},t)=\left(\frac{\delta f}{\delta t}\right)_{\text{coll.}}^{\text{QBGK}}=-\frac{(f-f^{(0)})}{\tau}, \tag{3}$$

where $f^{(0)}$ is the quantum equilibrium distribution function,

$$f^{(0)}(\vec{p},\vec{x},t)=\left\{\exp\left[\frac{(\vec{p}-m\vec{U}(\vec{x},t))^2}{2mk_{\text{B}}T(\vec{x},t)}-\mu(\vec{x},t)/k_{\text{B}}T(\vec{x},t)\right]+\theta\right\}^{-1}, \tag{4}$$

i.e., either the Bose–Einstein distribution or the Fermi–Dirac distribution and τ is the relaxation time which is in general depending on the macroscopic variables. In Eq. (4), k_{B} is the Boltzmann constant, $\vec{U}(\vec{x},t)$ the mean velocity, $T(\vec{x},t)$ the gas temperature, and $\mu(\vec{x},t)$ is the chemical potential. Extension and generalization of this BGK model to other systems are also commonly used with appropriate definition of the relaxation times. In this work, for convenience, we call the BGK model with quantum equilibrium distribution as QBGK model.

2.1. Connection to hydrodynamic equations

The hydrodynamic conservation laws are obtained by multiplying Eq. (1) by $1,\vec{p}$, or $\vec{p}^2/2m$, and then integrating the resulting equations over all $\vec{p}$. The integrals of the collision terms in all three cases vanish automatically and we have the differential conservation laws for the conserved macroscopic quantities, i.e., the particle number density $n(\vec{x},t)$, the momentum density, $\vec{J}=m\vec{j}$, and the energy density, $E(\vec{x},t)$, as follows:

$$\frac{\partial n(\vec{x},t)}{\partial t}+\nabla_{\vec{x}}\cdot n\vec{U}(\vec{x},t)=0, \tag{5}$$

$$nm\frac{\partial\vec{U}(\vec{x},t)}{\partial t}+(\vec{U}\cdot\nabla_{\vec{x}})\vec{U}+\frac{\partial P_{\alpha\beta}}{\partial x_\beta}+n\frac{\partial V}{\partial x_\alpha}=0, \tag{6}$$

$$\frac{\partial E(\vec{x},t)}{\partial t}+\nabla_{\vec{x}}\cdot(E\vec{U})+\nabla_{\vec{x}}\cdot\vec{Q}+D_{\alpha\beta}P_{\alpha\beta}=0. \tag{7}$$

The definitions of the number density, number density flux, and energy density are given, respectively, by

$$n(\vec{x},t)=\int\frac{\mathrm{d}\vec{p}}{h^3}f(\vec{p},\vec{x},t), \tag{8}$$

$$\vec{j}(\vec{x},t)=\int\frac{\mathrm{d}\vec{p}}{h^3}\frac{\vec{p}}{m}f(\vec{p},\vec{x},t)=n(\vec{x},t)\vec{U}(\vec{x},t), \tag{9}$$

$$E(\vec{x},t)=\int\frac{\mathrm{d}\vec{p}}{h^3}\frac{\vec{p}^2}{2m}f(\vec{p},\vec{x},t). \tag{10}$$

Other higher-order moments such as stress tensor and the heat flux vector can also be defined and they are, respectively, given by

$$P_{\alpha\beta}(\vec{x},t)=\int\frac{\mathrm{d}\vec{p}}{h^3}\left(\frac{p_\alpha}{m}-U_\alpha\right)\left(\frac{p_\beta}{m}-U_\beta\right)f(\vec{p},\vec{x},t), \tag{11}$$

$$Q_\alpha(\vec{x},t)=\int\frac{\mathrm{d}\vec{p}}{h^3}\frac{(\vec{p}-m\vec{U})^2}{2m}\left(\frac{p_\alpha}{m}-U_\alpha\right)f(\vec{p},\vec{x},t). \tag{12}$$

In Eq. (7), $D_{\alpha\beta}=(\partial U_\alpha/\partial x_\beta+\partial U_\beta/\partial x_\alpha)/2$ is the rate of strain tensor. The main objective of the present work is to derive a class of high resolution gas-kinetic schemes for solving the set of equations, Eqs. (5)–(7) based on the first-order expansion of semiclassical BGK-Boltzmann equation.

2.2. Zeroth-order solution

Several formal solution procedures which generalize the Chapman–Enskog method [4] to solve Eq. (1) have been presented by Gardner [9], Nikuni and Griffin [16], and Gardner and Ringhofer [10], where the first and second approximations of the distribution function and expressions for the viscosity and heat conductivity coefficients were given. If we consider only the lowest order (first approximation) of solution of the above Boltzmann equation and require that the collision term in Eq. (1) be zero, i.e., $(\delta f/\delta t)_{\text{coll.}}^{\text{UU}}=0$. The lowest-order solution to Eq. (1) (with $\nabla V(\vec{x},t)=0$), for one spatial dimension is given by

$$f^{(0)}(c_x,x,t)=\frac{1}{z^{-1}\mathrm{e}^{m[(c_x-U_x)^2+\xi^2]/2k_{\text{B}}T(x,t)}+\theta}=\frac{1}{z^{-1}\mathrm{e}^{\lambda((c_x-U_x)^2+\xi^2)}+\theta}, \tag{13}$$

where $z(x,t) = e^{\mu(x,t)/k_B T(x,t)}$ is the fugacity, $c_i = p_i/m, \xi^2 = c_y^2 + c_z^2, \lambda = m/2k_B T$, and $U_x(x,t)$ is the mean velocity component. For the local equilibrium quantum distribution, one can obtain these macroscopic quantities in closed form in terms of the Fermi or Bose functions, thus the dynamic behaviors can be simulated, for example, see [26,12]. In this work, our main aim is to derive the gas-kinetic BGK method for gas of particles of arbitrary statistics which is the direct generalization of Xu's work [23] for classical gas. We neglect the mean field potential $V(\vec{x},t)$ for simplicity. It is noted that in the presence of a non-uniform external potential the equilibrium distribution function will not be the Bose–Einstein or the Fermi–Dirac distribution but with a much more involved expression [9–11,18]. For one-dimensional flows, the molecular velocity components of the other two directions was taken as internal variables. With this zeroth-order distribution, one can work out all the hydrodynamic variables Eqs. (8)–(10), see [13]. For example, the number density $n(x,t)$ is given by

$$n(x,t) = \int_{-\infty}^{\infty} \frac{d^3p}{h^3} f^{(0)} = \int_{-\infty}^{\infty} f^{(0)}\, d\Xi = \frac{Q_{3/2}(z)}{\Lambda^3}, \quad d\Xi = d^3p/h^3, \tag{14}$$

where $\Lambda = \sqrt{\frac{\lambda h^2}{\pi m^2}}$ is the de Broglie thermal wavelength and h is the Planck constant, the momentum $\vec{j}(x,t)$ in x direction,

$$j_x(x,t) = \int_{-\infty}^{\infty} c_x f^{(0)} d\Xi = n(x,t) U_x(x,t) \tag{15}$$

and the energy density $E(x,t)$,

$$E(x,t) = \int_{-\infty}^{\infty} \frac{(p_x^2 + m^2\xi^2)}{2m} f^{(0)} d\Xi = \frac{3mQ_{5/2}(z)}{4\lambda\Lambda^3} + \frac{1}{2} mnU_x^2. \tag{16}$$

The function Q_n represents for either the Bose–Einstein or Fermi–Dirac function of order n which is defined as

$$Q_n(z) \equiv \frac{1}{\Gamma(n)} \int_0^{\infty} \frac{x^{n-1}}{z^{-1}e^x + \theta}\, dx = \sum_{l=1}^{\infty} (-\theta)^{l-1} \frac{z^l}{l^n}, \tag{17}$$

where $\Gamma(n)$ is the Gamma function. Furthermore, the corresponding hydrodynamic equations integrated from the zeroth-order solution give the "quantum Euler equations" in which the heat flux and the shear viscosity are zero in this case.

2.3. Chapman–Enskog expansion of quantum BGK

The zeroth-order distribution can be further extended to the next approximation of first-order distribution. The first-order solutions in classical and quantum cases will depict distinction and difference due to different zeroth-order solutions. The first-order distribution functions of classical and quantum gases from the Chapman–Enskog procedure assume, respectively, the form

$$f_c^{(1)} = f_c^{(0)}(1 + \quad_c), \tag{18}$$

$$f^{(1)} = f^{(0)}[1 + \quad_q(1 - \theta f^{(0)})], \tag{19}$$

where $f_c^{(0)}$ corresponds the classical distribution (Maxwell–Boltzmann distribution, $\theta = 0$) and $\quad$ is determined by the type of the collision model. The subscripts c and q denote the classical and quantum gases, respectively. The first-order solutions to BGK and QBGK equation share the same form as $f^{(1)} = f^{(0)} - \tau D f^{(0)}$. In classical BGK model, the first-order distribution function is

$$f_c^{(1)} = f_c^{(0)} \left[1 - \tau \left\{ \frac{c' \cdot \nabla T}{T} \left[\frac{mc'^2}{2k_B T} - \frac{5}{2} \right] + \frac{m}{k_B T} \frac{\partial U_\mu}{\partial x_\upsilon} (c'_\mu c'_\upsilon - \frac{1}{3}\delta_{\mu\upsilon} c'^2) \right\} \right]. \tag{20}$$

This first-order distribution means the deviation away from the equilibrium solution. If we integrate Eq. (3) by definitions of Eqs. (8)–(12), we can get the corresponding hydrodynamic Navier–Stokes equations. The corresponding viscosity and thermal conductivity are given by $\eta = \tau n k_B T = \tau P$, and $\kappa = \tau \frac{5k_B}{2m} n k_B T = \tau \frac{5k_B}{2m} P$, where η is the dynamical viscosity and P is the gas pressure. The viscosity and the conductivity estimated by BGK model will depend on the relaxation time and the corresponding pressure. Furthermore, the Prandtl number in this classical model is equal to 1 for monatomic gases. In the QBGK model, we use the same procedures with $f = f^{(0)} - \tau D f^{(0)}$ and

$$\begin{aligned} Df^{(0)} &= c'_i \frac{\partial \ln z}{\partial x_i} + \frac{(c_i - U_i)^2}{k_B T} \left(c'_i \frac{\partial T}{\partial x_i} - \frac{2}{3} T \frac{\partial U_i}{\partial x_i} \right) - \frac{1}{k_B T} \left(\frac{\partial}{\partial t} + c_i \frac{\partial}{\partial x_i} \right) \frac{(c_i - U_i)^2}{2m} \\ &= c'_i \frac{\partial \ln z}{\partial x_i} + \frac{mc'^2}{k_B T^2} \left(c'_i \frac{\partial T}{\partial x_i} - \frac{2}{3} T \frac{\partial U_i}{\partial x_i} \right) + \frac{mc'}{k_B T} \left(\frac{\partial U}{\partial t} + c_i \frac{\partial U}{\partial x_i} \right). \end{aligned}$$

Replace the time derivative by zeroth-order conservation laws, the first-order solution of QBGK equation

$$\begin{aligned} f^{(1)} &= f^{(0)} - \tau D f^{(0)}, \\ D f^{(0)} &= f^{(0)}(1-\theta f^{(0)})\left[\frac{c'\cdot\nabla T}{T}\left[\frac{mc'^2}{2k_B T}-\frac{5Q_{\frac{5}{2}}(z)}{2Q_{\frac{3}{2}}(z)}\right]+\frac{m}{k_B T}\frac{\partial U_\mu}{\partial x_\upsilon}\left(c'_\mu c'_\upsilon-\frac{c'^2}{3}\delta_{\mu\upsilon}\right)\right] \end{aligned} \tag{21}$$

The viscosity and thermal conductivity for a quantum gas can be also derived using the same argument as those in classical gas and they are given respectively by

$$\eta = \tau n k_B T \frac{Q_{5/2}(z)}{Q_{3/2}(z)} = \tau P, \tag{22}$$

$$\kappa = \tau \frac{5k_B}{2m} n k_B T\left[\frac{7}{2}\frac{Q_{7/2}(z)}{Q_{3/2}(z)}-\frac{5}{2}\frac{Q^2_{5/2}(z)}{Q_{3/2}(z)}\right]. \tag{23}$$

It is found that the viscosity and conductivity derived from QBGK model depend not only on the relaxation time but also on the Bose or Fermi functions. The physical meaning of z will be illustrated later. The Prandtl number of the QBGK model is z dependent and it will not equal to 1 when z is not small enough. For similar results from linearized semiclassical Boltzmann equation, see [16]. The hydrodynamic equations from the first-order distribution of QBGK correspond to the "quantum Navier–Stokes equation".

2.4. Classical limit of quantum gases

After introducing the zeroth and first-order solutions of classical and quantum BGK equations, we next describe the connections between them. It is well known that the classical Maxwell–Boltzmann distribution is the limiting case of both Bose–Einstein and Fermi–Dirac distributions. The macroscopic properties such as pressure, density, viscosity, etc., that evaluated according to quantum statistics are different from those of classical one, but in certain conditions (in the classical limit) the behavior of the quantum gas will be the same as the classical one. First, in the limit $z^{-1}e^{\lambda(\vec{c}-\vec{U})^2} \gg 1$, the quantum distribution function becomes

$$f^{(0)}(c_x, x, t) = z e^{-\lambda(\vec{c}-\vec{U})^2}. \tag{24}$$

For the Maxwell–Boltzmann distribution, the number density is represented as

$$\begin{aligned} f_c^{(0)} &= n_{cl}\left(\frac{h^2\lambda}{m^2\pi}\right)^{3/2} e^{-\lambda(\vec{c}-\vec{U})^2} = n_{cl}\Lambda^{3/2} e^{-\lambda(\vec{c}-\vec{U})^2}, \\ n_{cl} &= \int f^{(0)}_{\text{classical}}\, d^3p/h^3 = \frac{z}{\Lambda^3}. \end{aligned} \tag{25}$$

Then we have

$$z = n_{cl}(h^2/2\pi m k_B T)^{3/2} = n_{cl}\Lambda^3, \tag{26}$$

where n_{cl} is the number density of particles and z can be interpreted as the ratio of Λ^3 to average volume occupied by particles. When z is small, it means the order of spatial dimension is larger than the thermal wavelength and we can neglect the degeneracy effect of particles. For large z, the degeneracy effect is important because the order of thermal wavelength is comparable to the spatial dimension. Moreover, the thermal wavelength is proportional to $T^{-1/2}$, this means when the density is in normal condition this effect will be obvious especially in the low temperature. In summary, when $z \to 0$ the quantum distribution will coincide with the classical one, and the physical explanation is that the length dimension of particle is larger than the particle de Broglie wavelength. The wave property will not be important. When z is considerably large, the two length scales become comparable and one cannot omit the quantum effect anymore. So, we can think of the fugacity z as an indication of the degree of degeneracy. The fugacity z has some restrictions in two different quantum distributions. In the case of Boson, z should not exceed 1 because of the non-negative density, and in the Fermion case there are no such restrictions on z.

Finally, the actual correction values of the number density, shear viscosity and thermal conductivity are plotted in Fig. 1. From Fig. 1, one finds that the BE and FD curves overlap with MB curve in the $z \to 0$ limit, this means the classical statistics could only work under high temperature or low chemical potential conditions and is the classical limit of quantum statistics. One of the computational examples given later will illustrate and compare this classical limit.

3. The gas-kinetic quantum BGK scheme

To illustrate the derivation of the gas-kinetic quantum BGK scheme for quantum gas flows, we first consider the formulation in one space dimension in Cartesian coordinates. Divide the computational space into a number of cells of size Δx_i.

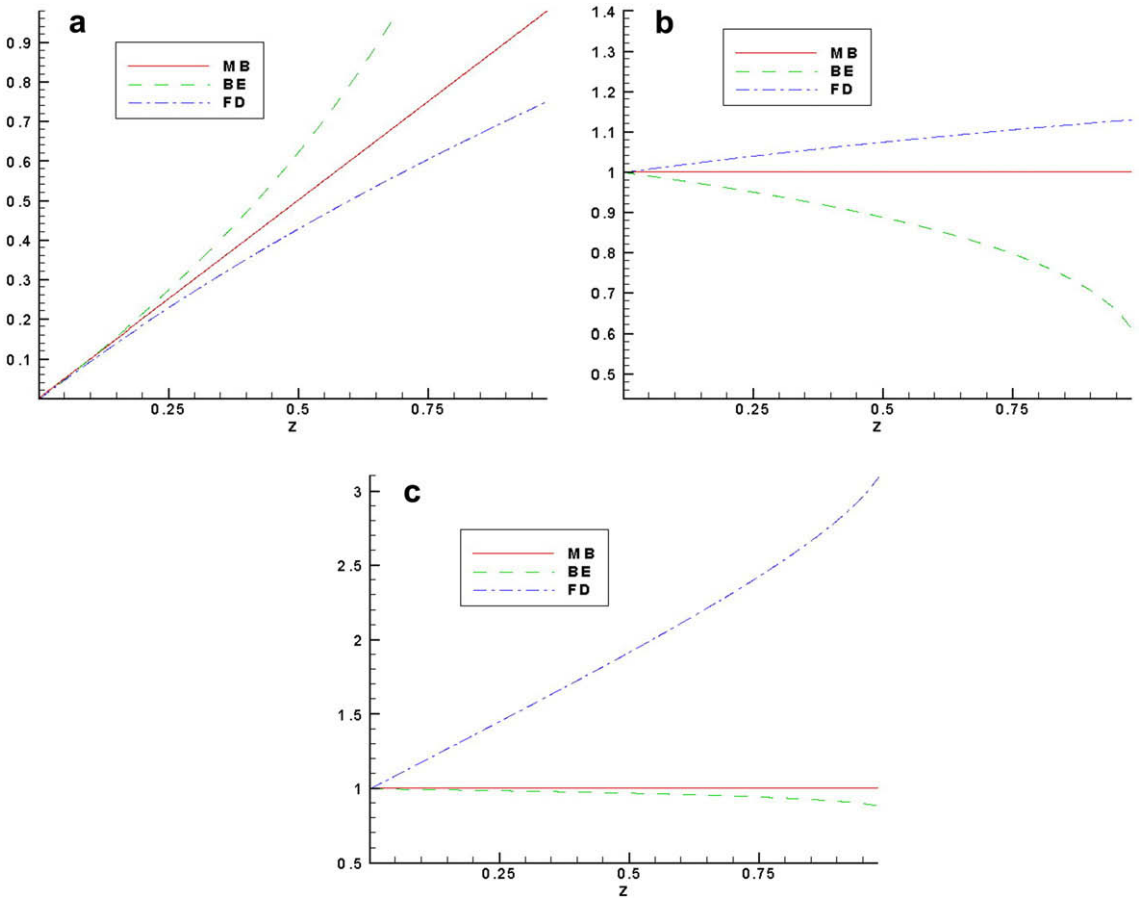

Fig. 1. The values of quantum functions for different statistics: (a) number density, $n(z)$; (b) η/η_c; (c) κ/κ_c.

Without loss of generality, we assume uniform cells with length Δx. The local state of gas in each cell i at any time t is specified by $\mathbf{W}_i = (n, nu_x, \epsilon)_i^{\mathrm{T}}$, which are the mass density, x-momentum density, and the energy density, respectively. The QBGK model in 1-D case $\vec{U} = U(x,t)\vec{i}$ is

$$\frac{\partial f(x,\vec{c},t)}{\partial t} + c_x \frac{\partial f(x,\vec{c},t)}{\partial x} = \frac{f^{(0)} - f(x,\vec{c},t)}{\tau}. \tag{27}$$

The relaxation time in this work is assumed to be particle velocity independent. Although the effect of collision is simplified in QBGK model, it still retains the main character of collision. More rigorous theoretical derivation of the physical relaxation time for quantum Boltzmann equation is needed such as the Wigner-BGK equation by Degond and Ringhofer [7]. No matter how we model the process of collision, the conservation of mass, momentum and energy need to be satisfied all the time. This is called the compatibility condition. In the constant relaxation time QBGK model, the compatibility condition is

$$\int (f - f^{(0)})\phi \, \mathrm{d}\Xi \, \mathrm{d}t = 0, \quad \phi = \begin{bmatrix} 1 \\ c_x \\ \frac{1}{2}m(c_x^2 + c_y^2 + c_z^2) \end{bmatrix}. \tag{28}$$

One of the advantages of using BGK or QBGK model is that it can be solved analytically by following the characteristic line. For a given initial condition $f_0(x,\vec{c})$, the solution of QBGK equation, Eq. (27), describes how the particle distribution evolves with time under QBGK model, and is given by

$$f(x,t,c_x) = \frac{1}{\tau}\int_0^t g(x',t',c_x)\mathrm{e}^{(t-t')/\tau}\,\mathrm{d}t' + \mathrm{e}^{-t/\tau} f_0(x - c_x t), \tag{29}$$

where f_0 is the initial gas distribution function f at the beginning of each time step ($t = 0$), g is the equilibrium distribution function, and $x' = x - c_x(t - t')$ is the trajectory of a particle motion. Both the unknown functions g and f_0 must be specified in Eq. (29) in order to obtain the solution f. We follow the idea of Xu [23] to find the distribution function at cell inter-

face ($x = x_{j+1/2}$) and extend the method to a quantum BGK flow solver. Both the initial gas distribution function and the equilibrium state in the QBGK model are evaluated based on the linear distribution of macroscopic flow variables. The initial gas distribution function, f_0, is assumed to be in a non-equilibrium state obtained from the first-order Chapman–Enskog expansion of the BGK model and it assumes the form

$$f_0(x,t) = \begin{cases} f_l^{(0)} - \tau D f_l^{(0)}, & x < 0, \\ f_r^{(0)} - \tau D f_r^{(0)}, & x > 0, \end{cases} \tag{30}$$

where $f_l^{(0)}$ and $f_r^{(0)}$ are local quantum equilibrium distributions come from the initial reconstruction and $\tau D f_l^{(0)}$ and $\tau D f_r^{(0)}$ account for the deviation of a distribution function away from equilibrium. The detail will be given in the following subsection. After obtaining f_0, the equilibrium state g is assumed to take the following form

$$g(x',t') = g_0 - c_x(t-t')\bar{a}^l g_0' \overline{H}(c_x) - c_x(t-t')\bar{a}^r g_0' H(c_x) + \overline{A}t', \tag{31}$$

where $H(x)$ is the Heaviside function, $\overline{H}(x) \equiv 1 - H(x)$, g_0 is a local equilibrium distribution located at $x = 0$ and g_0' denotes the first-order derivative of g_0. Even though g is continuous at $x = 0$, it may have different slopes at $x < 0$ and $x > 0$ regions. In Eq. (31), $\bar{a}^l, \bar{a}^r$ and $\overline{A}$ are related to the derivatives of an equilibrium distribution in time and space. The gas is out of equilibrium automatically by virtue of a spatial distribution of macroscopic quantities such as the gradients of density, velocity and temperature.

It is noted that the non-equilibrium parts have no direct contribution to the conservative variables, i.e.,

$$\int D f_l^{(0)} \phi \, \mathrm{d}\Xi = 0, \quad \int D f_r^{(0)} \phi d\Xi = 0. \tag{32}$$

The details of constructing the initial gas distribution f_0 and the equilibrium state g are given separately below.

3.1. Initial distribution f_0

First, the first-order solution involves both the derivatives with respect to time and to space of the equilibrium solution. Unlike the classical Maxwellian exponential form, the spatial derivative of quantum equilibrium distribution is given by

$$\partial_x f^{(0)} = (a_1 + a_2 c_x + a_3 m(c_x^2 + \xi^2)/2) f^{(0)}(1 - \theta f^{(0)}) = (a_1 + a_2 c_x + a_3 m(c_x^2 + \xi^2)/2) f'^{(0)} = a^\alpha f'^{(0)} = a_\alpha \phi_\alpha f'^{(0)}, \tag{33}$$

where

$$a_1 = -U^2 \partial_x \lambda - 2\lambda U \partial_x U + z^{-1}\partial_x z, \quad a_2 = 2\lambda \partial_x U + 2U\partial_x \lambda, \quad a_3 = -2\partial_x \lambda \tag{34}$$

and

$$f'^{(0)} = f^{(0)}(1 - \theta f^{(0)}) = z^{-1} \mathrm{e}^{\lambda[(c_x - U)^2 + \xi^2]} / (z^{-1} \mathrm{e}^{\lambda[(c_x - U)^2 + \xi^2]} + \theta)^2. \tag{35}$$

Similarly, the expression for $\partial_t f^{(0)}$ can be obtained and we have

$$\partial_t f^{(0)} = A_\alpha \phi_\alpha f'^{(0)}. \tag{36}$$

Then, we have the first-order expansion of the distribution function as

$$f^{(1)} = f^{(0)} - \tau \cdot (A_\alpha \phi_\alpha + c_x a_\beta \phi_\beta) f'^{(0)}. \tag{37}$$

The definition of A_α is similar to a_α above, except it stands for time derivatives. Using Taylor's expansion and neglecting the high order terms, one approximates $f_0(x - c_x t)$ by

$$f_0(x_0 = x - c_x t) = f^{(1)}(x,t) + (x_0 - x) f^{(0)}(x,t) + \mathrm{O}(x^2). \tag{38}$$

Next, for a high resolution scheme, the reconstruction techniques are used to interpolate the cell averaged number, momentum, and energy densities. Simple polynomial expansion usually generates spurious overshoot or undershoot, or even oscillations if large variations in flow data are present initially. One of the most successful and reliable interpolation techniques known so far is the total variation diminishing (or non-increasing) method. For quantum BGK methods, the reconstruction techniques are applied to the conservative variables directly. The cell averaged mass, momentum, and energy densities are denoted by $\mathbf{W}_j$ and its interpolated value in cell j is $\overline{\mathbf{W}}_j(x)$, where $\overline{\mathbf{W}}_j(x_{j-1/2})$ and $\overline{\mathbf{W}}_j(x_{j+1/2})$ are two pointwise values on the left and right interfaces at the locations $x_{j-1/2}$ and $x_{j+1/2}$ in cell j. To second-order spatial accuracy, the interpolated value in the jth cell can be formally written as

$$\overline{\mathbf{W}}_j(x) = \mathbf{W}_j + L(s_{j+}, s_{j-})(x - x_j) \quad \text{for } x_{j-1/2} \leqslant x \leqslant x_{j+1/2}. \tag{39}$$

For the nonlinear van-Leer limiter, one has

$$L(s_{j+}, s_{j-}) = (\mathrm{sign}(s_{j+}) + \mathrm{sign}(s_{j-}))\frac{|s_{j+}||s_{j-}|}{|s_{j+}| + |s_{j-}|}, \tag{40}$$

$$s_{j+} = \frac{W_{j+1} - W_j}{x_{j+1} - x_j}, \quad s_{j-} = \frac{W_j - W_{j-1}}{x_j - x_{j-1}}. \tag{41}$$

The idea of interpolating separately in the regions $x \leqslant x_{j+1/2}$ and $x \geqslant x_{j+1/2}$ originates from the following physical consideration. For a non-equilibrium gas flow, since the cell size is usually much larger than the thickness of a discontinuity, physical quantities can change dramatically in space. For example, across a shock front, upstream and downstream gas distributions could be two different Bose–Einstein (or Fermi–Dirac) distributions. Therefore, we need to split f_0 accordingly to capture this possible physical reality, i.e., Eq. (30).

In the reconstruction stage described above, we have obtained $\hat{n}_j(x), \hat{n}_j\widehat{U}_j(x)$ and $\hat{\epsilon}_j(x)$ constructed in each cell $x_{j-1/2} \leqslant x \leqslant x_{j+1/2}$. The left and right macroscopic states at the cell interface $x_{j+1/2}$ are

$$\overline{\mathbf{W}}_j\left(x_{j+\frac{1}{2}}\right) = \begin{pmatrix} \hat{n}_j\left(x_{j+\frac{1}{2}}\right) \\ \hat{n}_j\widehat{U}_j\left(x_{j+\frac{1}{2}}\right) \\ \hat{\epsilon}_j\left(x_{j+\frac{1}{2}}\right) \end{pmatrix}, \quad \overline{\mathbf{W}}_{j+1}\left(x_{j+\frac{1}{2}}\right) = \begin{pmatrix} \hat{n}_{j+1}\left(x_{j+\frac{1}{2}}\right) \\ \hat{n}_{j+1}\widehat{U}_{j+1}\left(x_{j+\frac{1}{2}}\right) \\ \hat{\epsilon}_{j+1}\left(x_{j+\frac{1}{2}}\right) \end{pmatrix}. \tag{42}$$

By using the relation between the gas distribution function f and the macroscopic variables, at the cell interface $x_{j+\frac{1}{2}}$, we have

$$\int \phi f_l^{(0)}\,\mathrm{d}\Xi = \overline{\mathbf{W}}_j\left(x_{j+\frac{1}{2}}\right), \quad \int \phi a^l f_l'^{(0)}\,\mathrm{d}\Xi = \frac{\overline{\mathbf{W}}_j\left(x_{j+\frac{1}{2}}\right) - \overline{\mathbf{W}}_j(x_j)}{\Delta x^-}, \tag{43}$$

$$\int \phi f_r^{(0)}\,\mathrm{d}\Xi = \overline{\mathbf{W}}_{j+1}\left(x_{j+\frac{1}{2}}\right), \quad \int \phi a^r f_r'^{(0)}\,\mathrm{d}\Xi = \frac{\overline{\mathbf{W}}_{j+1}(x_{j+1}) - \overline{\mathbf{W}}_{j+1}\left(x_{j+\frac{1}{2}}\right)}{\Delta x^+}, \tag{44}$$

where $\Delta x^- = x_{j+1/2} - x_j$ and $\Delta x^+ = x_{j+1} - x_{j+1/2}$. With the definition of quantum equilibrium distributions,

$$\begin{aligned} f_l^{(0)} &= [z_l^{-1}\exp\lambda_l\{(c_x - U_l)^2 + \xi^2\} + \theta]^{-1}, \\ f_r^{(0)} &= [z_r^{-1}\exp\lambda_r\{(c_x - U_r)^2 + \xi^2\} + \theta]^{-1}, \end{aligned} \tag{45}$$

all the parameters (n_l, U_l, λ_l) and (n_l, U_l, λ_l) in $f_l^{(0)}$ and $f_r^{(0)}$, respectively, can be uniquely determined.

It is noted that the way to transform macroscopic variables $\mathbf{W}$ to fugacity z is by numerically solving the following equation,

$$\chi_3 = 2\epsilon - 3(n/Q_{3/2}(z))^{5/3}Q_{5/2}(z) - j^2/n = 0. \tag{46}$$

Once $f_l^{(0)}$ and $f_r^{(0)}$ have been obtained (as well as $f_l'^{(0)}$ and $f_r'^{(0)}$), the slopes a^l and a^r can be evaluated by solving matrix equations. After obtaining a^l and a^r, the parameters A^l and A^r in f_0 can be found from Eq. (32).

3.2. The equilibrium distribution g

The equilibrium function $g(x', t')$ is constructed from the Taylor expansion of g_0. And g_0 is determined by taking the limit $t \to 0$ to the solution of Eq. (29)

$$\int_{c_x>0}\int \phi_\alpha f_l^{(0)}\,\mathrm{d}\Xi + \int_{c_x<0}\int \phi_\alpha f_r^{(0)}\,\mathrm{d}\Xi = \mathbf{W}_{0j} = \int\int g_0\phi_\alpha\,\mathrm{d}\Xi. \tag{47}$$

The macroscopic state $\mathbf{W}_{0j}$ on cell interface between j cell and $j+1$ cell is constructed through the above equation. Since g_0 is the local equilibrium distribution, it can be uniquely determined from the corresponding macroscopic variables $\mathbf{W}_0$. If we define $x = 0$ at the cell interface, then $g(x', t')$ can be approximated by

$$g(x', t') = g_0 + (x' - x)\partial_x g_0 H(x) + (x' - x)\partial_x g_0\overline{H}(x) + t'\overline{A}. \tag{48}$$

Next, the corresponding coefficients $\bar{a}^l$ and $\bar{a}^r$ are spatial derivatives of g_0 on the left $(x < 0)$ and right $(x > 0)$ sides of the cell interface, respectively. These coefficients are obtained in the following way,

$$\int \phi_\alpha \bar{a}^l g_0\,\mathrm{d}\Xi = \frac{\overline{\mathbf{W}}_{0j}\left(x_{j+\frac{1}{2}}\right) - \overline{\mathbf{W}}_j(x_j)}{\Delta x^-}, \tag{49}$$

$$\int \phi_\alpha \bar{a}^r g_0\,\mathrm{d}\Xi = \frac{\overline{\mathbf{W}}_{j+1}(x_j) - \overline{\mathbf{W}}_{0j}\left(x_{j+\frac{1}{2}}\right)}{\Delta x^+}. \tag{50}$$

Note that Δx^- is the distance from cell interface to the left cell center and Δx^+ is the distance from cell interface to the right cell center.

By this time, we have determined all parameters in the initial gas distribution function f_0 and the equilibrium state g at the beginning of each time step $t = 0$ and we are ready to calculate the time-varying distribution function at the cell interface $f(x_{j+1/2}, t, c_x)$ in an explicit and analytical form.

3.3. The solution distribution function of QBGK

Finally, the time varying distribution function on the cell interface can be derived by substituting Eqs. (30) and (31) into Eq. (29)

$$\begin{aligned} f(x_{j+1/2}, t, c_x) = {} & (1 + C_1)g_0 + t\overline{A}g_0' + C_2 c_x[\bar{a}^l H(c_x) + \bar{a}^r \overline{H}(c_x)]g_0' + C_3[H(c_x)f_l^{(0)} + \overline{H}(c_x)f_r^{(0)}] + C_4 c_x[a^l H(c_x)f_l'^{(0)} \\ & + a^r \overline{H}(c_x)f_r'^{(0)}] + C_5[A^l H(c_x)f_l'^{(0)} + A^r \overline{H}(c_x)f_r'^{(0)}] + C_6\overline{A}g_0', \end{aligned} \tag{51}$$

where

$$\begin{aligned} & C_1 = -\mathrm{e}^{-t/\tau}, \quad C_2 = -\tau + (t + \tau)\mathrm{e}^{-t/\tau}, \quad C_3 = \mathrm{e}^{-t/\tau}, \\ & C_4 = -(t + \tau)\mathrm{e}^{-t/\tau}, \quad C_5 = -\tau\mathrm{e}^{-t/\tau}, \quad C_6 = \tau(-1 + \mathrm{e}^{-t/\tau}). \end{aligned} \tag{52}$$

The coefficient functions $C_i(t, \tau)$ are function of t and τ. The remaining unknown coefficients in Eq. (51) are $\overline{A}$, and it can be determined by imposing a condition by generalizing the compatibility condition Eq. (28) on the cell interface in one whole time step

$$\int_0^{\triangle t} \int (f - f^{(0)})\phi \,\mathrm{d}\Xi \,\mathrm{d}t = 0. \tag{53}$$

It is noted that the above distribution function $f(x_{j+1/2}, t, c_x)$ is the main result of the present work and the classical counterpart of Xu's work can be recovered from this equation as one takes the classical limit.

Lastly, the time-dependent numerical fluxes across the cell interface can be computed as

$$F(x_{j+1/2}, t) = \begin{pmatrix} F_n \\ F_j \\ F_\epsilon \end{pmatrix}_{j+1/2} = \int c_x \phi_\alpha f(x_{j+1/2}, t, c) \,\mathrm{d}\Xi. \tag{54}$$

By integrating the above time-dependent numerical flux at the cell interface for the whole time step Δt, one gets the total mass, momentum and energy transport as follows:

$$F(x_{j+1/2}, t) = \sum_{i=1}^{6} F_i, \quad \gamma_i \equiv \frac{1}{\triangle t}\int_0^{\triangle t} C_i \,\mathrm{d}t, \tag{55}$$

where

$$\begin{aligned} F_1 &= (1 + \gamma_1)\int c g_0 \phi \,\mathrm{d}\Xi, \\ F_2 &= \gamma_2 \int c^2[\bar{a}^l H(c) + \bar{a}^r \overline{H}(c)]g_0'\phi \,\mathrm{d}\Xi, \\ F_3 &= \gamma_3 \int c[H(c)f_l^{(0)} + \overline{H}(c)f_r^{(0)}]\phi \,\mathrm{d}\Xi, \\ F_4 &= \gamma_4 \int c^2[a^l H(c)f_l'^{(0)} + a^r \overline{H}(c)f_r'^{(0)}]\phi \,\mathrm{d}\Xi, \\ F_5 &= \gamma_5 \int c[A^l H(c)f_l'^{(0)} + A^r \overline{H}(c)f_r'^{(0)}]\phi \,\mathrm{d}\Xi, \\ F_6 &= (\gamma_6 + \triangle t/2)\int c\overline{A}f_0'^{(0)}\phi \,\mathrm{d}\Xi. \end{aligned} \tag{56}$$

The computations of moments and the γ_s of each flux term are included in the Appendix.

Finally, a brief explanation of these fluxes is discussed. The F_1 and F_2 correspond to collision effect of BGK equation. The F_3 represents the evolutions of $f_l^{(0)}$ and $f_r^{(0)}$. The F_4 contains two different parts, one is from Taylor expansion of $f_0(x - ct)$ to first order and the other is from the spatial derivative of first-order solution $(Df^{(0)})$. The F_5 is the time derivative of first-order solution $Df^{(0)}$ and F_6 is the time derivative of g which satisfies the compatibility condition in one time step.

The present gas-kinetic QBGK scheme for quantum hydrodynamic transport can finally be expressed as

$$\mathbf{W}_j^{n+1} = \mathbf{W}_j^n - \frac{1}{\Delta x}\int_{t^n}^{t^n + \Delta t} [F(x_{j+1/2}, t) - F(x_{j-1/2}, t)] \,\mathrm{d}t. \tag{57}$$

This is a second-order accurate (both in time and space) TVD quantum hydrodynamic transport solver with viscosity and thermal conductivity effects taken into account.

4. Relaxation time of QBGK scheme

This section shall focus on the discussion of physical relaxation time which comes from empirical or some derivations according to the flow condition. Since different carriers can be considered in quantum BGK equation, the relaxation time should depend not only on gas dynamical problems but also on different physics problems. Important carrier scattering mechanisms can be identified and classified for common semiconductors. For example, the relaxation times for various scattering mechanisms of different carriers transport in semiconductor devices including electrons, holes and others have been proposed, see [15]. The conditions under which the relaxation time approximation is valid were also identified. In the present BGK or QBGK models, the relaxation time is related to viscosity ($\eta = \tau P$). The relaxation time in quantum case is modified with the pressure term $P_q = nk_BTQ_{5/2}(z)/Q_{3/2}(z)$, and is compared to the classical one $P_c = nk_BT$. That is

$$\tau_c = \frac{\eta}{nk_BT}, \quad \tau_q = \eta\frac{Q_{3/2}(z)}{nk_BTQ_{5/2}(z)}. \tag{58}$$

In most work of the BGK scheme, the relaxation time is determined by $\tau = \eta_0/P_0$, and P_0 is the corresponding pressure to the constructed state g_0 and $\eta_0 = \eta_0(T_0)$ is the viscosity which follows the power law or the Sutherland's formula. Here, another approach for defining relaxation time can also be employed which offers the advantage of easily calculated collision mechanics. The average velocity of the quantum gas particles is equal to

$$\bar{c} = \frac{\int cf\,d\xi}{\int f\,d\xi} = \sqrt{\frac{8k_BT}{m\pi}}\frac{Q_2(z)}{Q_{3/2}(z)} \tag{59}$$

and the mean free path can be approximated with $l_{MFP} = \frac{1}{\sqrt{2}n\pi d^2}$ where d is the effective diameter, e.g., variable hard sphere molecular model. With the mean free path and the average velocity, we can estimate the relaxation time

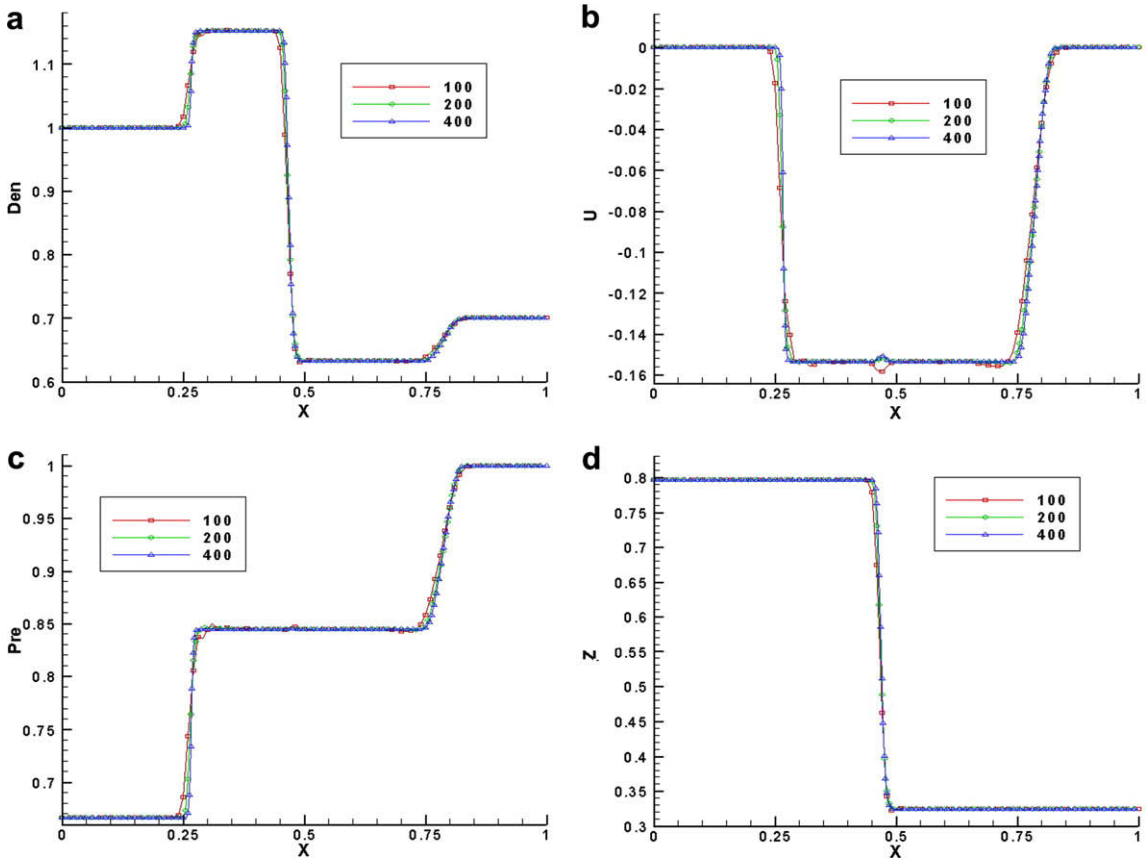

Fig. 2. Test of the grid convergence of gas-kinetic QBGK scheme (NS_2): (a) number density; (b) mean velocity; (c) pressure; (d) fugacity.

$$\tau_q = \frac{l_{MFP}}{\bar{c}} = \frac{1}{4n\mathrm{d}^2\pi}\sqrt{\frac{m}{k_B T}}\frac{Q_2(z)}{Q_{3/2}(z)}. \tag{60}$$

For a Boson gas, one can also use the shear viscosity derived by Nikuni and Griffin [16]. This viscosity is related to the scattering length a as

$$\eta_B = \frac{5}{16a^2}\left(\frac{mk_B T}{\pi}\right)^{1/2}\frac{\pi^{1/2}}{8I'_B(z)}g^2_{5/2}(z), \quad \tau_B = \eta_B/P_q, \tag{61}$$

where $I'_B(z)$ is a special function involving the local distribution function $f^{(0)}$, and was defined in [16].

After obtaining the viscosity, we know that in the QBGK equation $\tau_B = \eta_B/P_q$ and the relaxation time for a boson gas is thus obtained.

In the following numerical experiments, we shall consider four types of relaxation times. The first type is to assume $\tau = \text{const.}$ and we test different range of values of τ which are corresponding to different magnitudes of viscosity. The second type, called the physical relaxation time, is according to the expression of τ_q defined by Eq. (58). For numerical purpose, we also test a modified relaxation time similar to that used by Xu [23],

$$\tau_{mod} = \tau_{phys} + S_1\Delta t|p_L - p_R|/|p_L + p_R|, \tag{62}$$

where p_L and p_R are pressures constructed in the left and right sides of the cell interface, S_1 is a constant, and τ_{phys} is the physical relaxation time defined above. For $S_1 = 0$, we have simply $\tau_{mod} = \tau_{phys}$. The third type is defined by Eq. (60) using the gas particle mean free path and mean velocity. We also test different values of effective diameter d used in Eq. (60). The fourth type is for a Boson gas and the relaxation time is calculated according to Eq. (61) given by Nikuni and Griffin [16]. We also test different values of scattering length a used in Eq. (61).

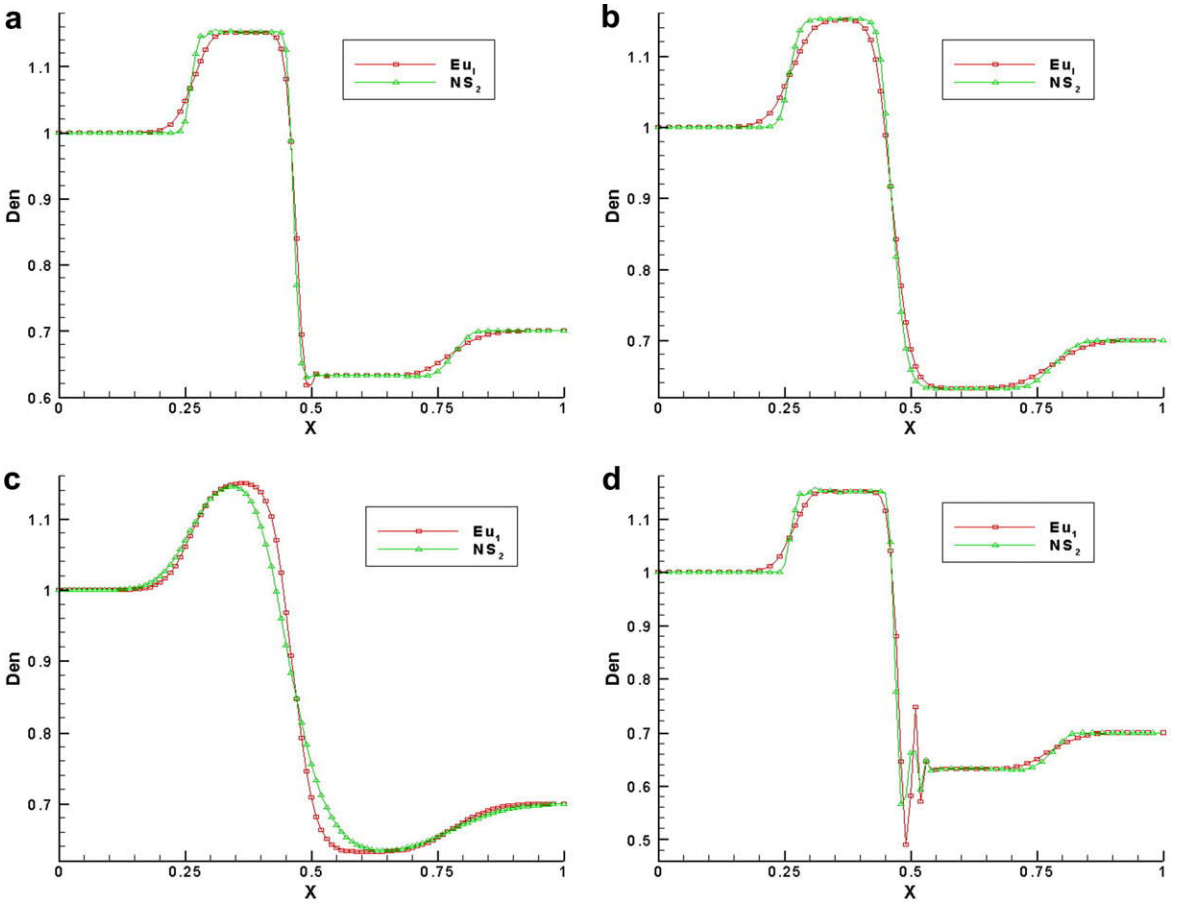

Fig. 3. Test of the spatial reconstruction, density profiles: (a) $\tau = 0.0001$; (b) $\tau = 0.001$; (c) $\tau = 0.01$; (d) $\tau = 10^{-10}$.

5. Numerical examples and discussions

In this section, we report some numerical examples to illustrate the performance of the present quantum gas-kinetic BGK schemes. For numerical validation and comparison purposes, we apply the numerical methods to one-dimensional quantum gas flows in a shock tube. The equations are non-dimensionalized by the following reference quantities

$$x_0 = h/(2\pi m k_B T_0)^{1/2}, \quad U_0 = \sqrt{k_B T_0/m}, \quad t_0 = \frac{x_0}{U_0}, \quad n_0 = \frac{1}{x_0^3}, \quad P_0 = m n_0 U_0^2,$$

where a reference mass is chosen for m. The total length of the shock tube is equal to 1 and the simulation output time is equal to 0.2. The CFL condition is $|U + 3.0 * S_p|_{max} \leqslant \Delta x/\Delta t$, and $S_p = \sqrt{5P/3\rho}$ is the sound speed. Unless specified otherwise, in most cases the macroscopic conditions of the left and right sides of the diaphragm in the shock tube are $(n_L, u_L, \epsilon_L) = (1.0, 0.0, 1.0)$ and $(n_R, u_R, \epsilon_R) = (0.7, 0.0, 1.5)$, respectively. These two states correspond to two different fugacities $z_L = 0.7971$ and $z_R = 0.3245$ in which the quantum effect of the gases is included. Generally the number of grids used is 100, CFL = 0.5, and the Boson gas is tested. Several issues regarding to the relaxation time resulting from different effective diameter, d and scattering length, a will be also examined here. We denote the gas-kinetic QBGK scheme with reconstruction using van Leer limiter as NS_2 which is a second-order accurate scheme in time and space for the quantum Navier–Stokes equations. For numerical comparison, in Examples 1–3, we assume constant relaxation time and the physical relaxation time will be used in Examples 4 and 5.

Example 1 (*Test of grid convergence*). The initial set up of the problem was described as above. This example refines the number of grids from 100 to 400. The initial conditions of the left and right states are specified as above for a Boson gas. The relaxation time is set to constant $\tau = 0.0001$. The numerical method used was NS_2. The results are shown in Fig. 2. The main features of a typical shock tube flow, namely, the shock wave, contact discontinuity and the expansion fan, are well represented. The grid convergence of the scheme is depicted.

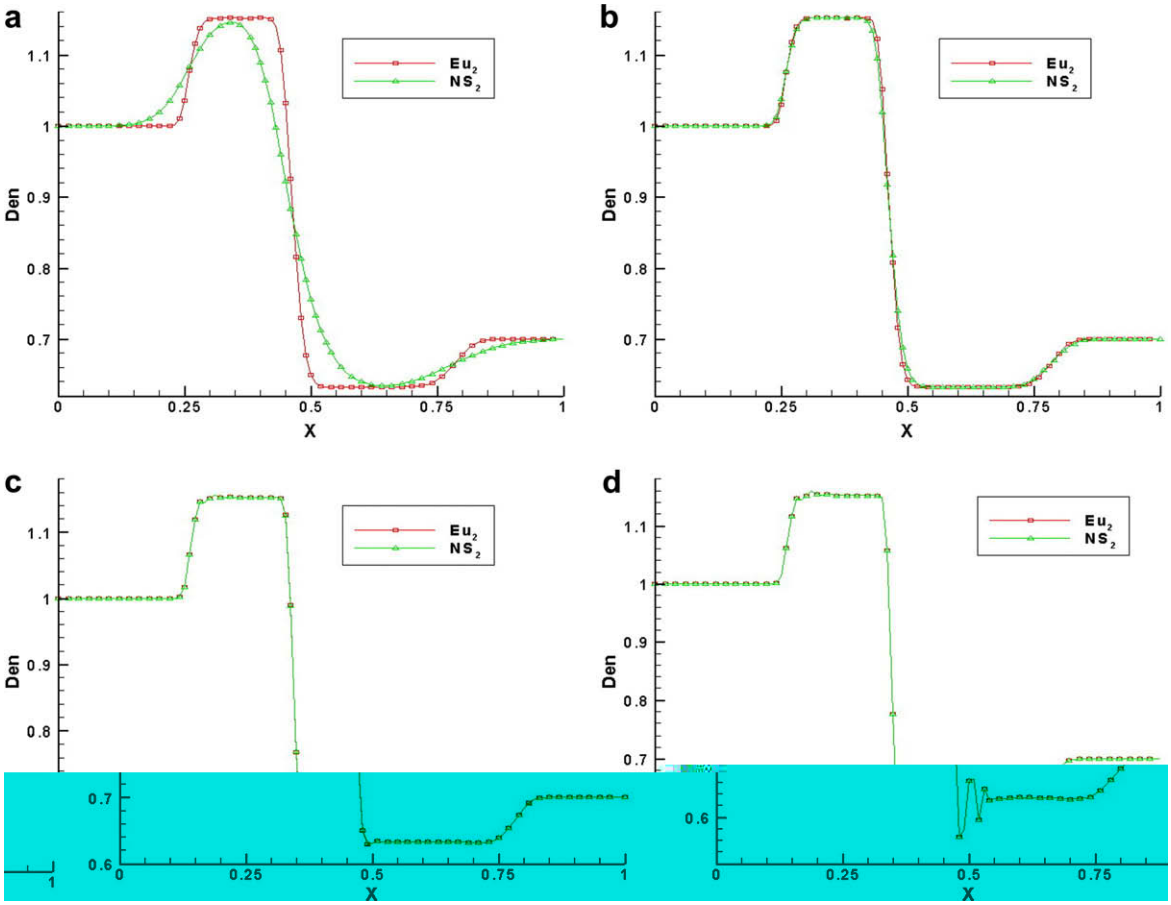

Fig. 4. Test of physical viscosity, density profile: (a) $\tau = 0.01$; (b) $\tau = 0.001$; (c) $\tau = 0.0001$; (d) $\tau = 10^{-10}$.

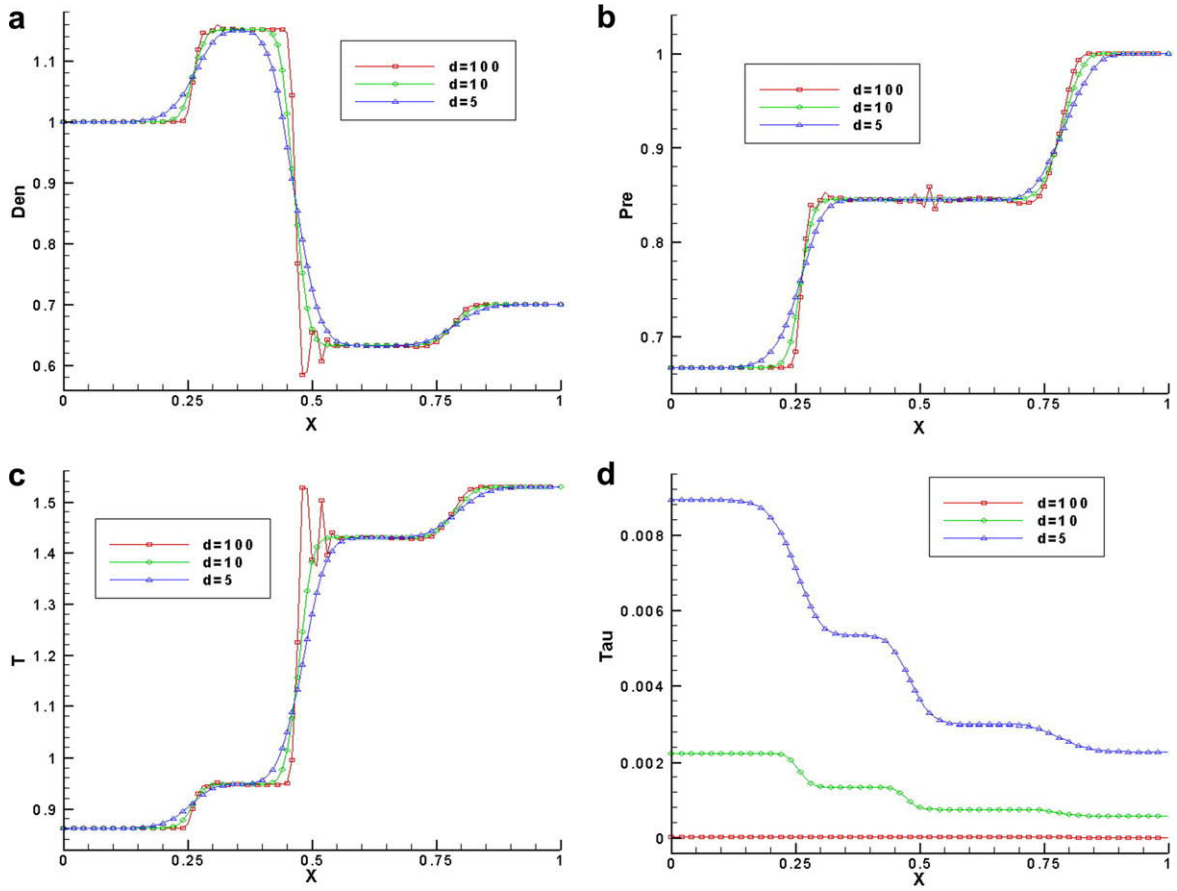

Fig. 5. Tests on different effective diameter: (a) density; (b) pressure; (c) temperature; (d) relaxation time.

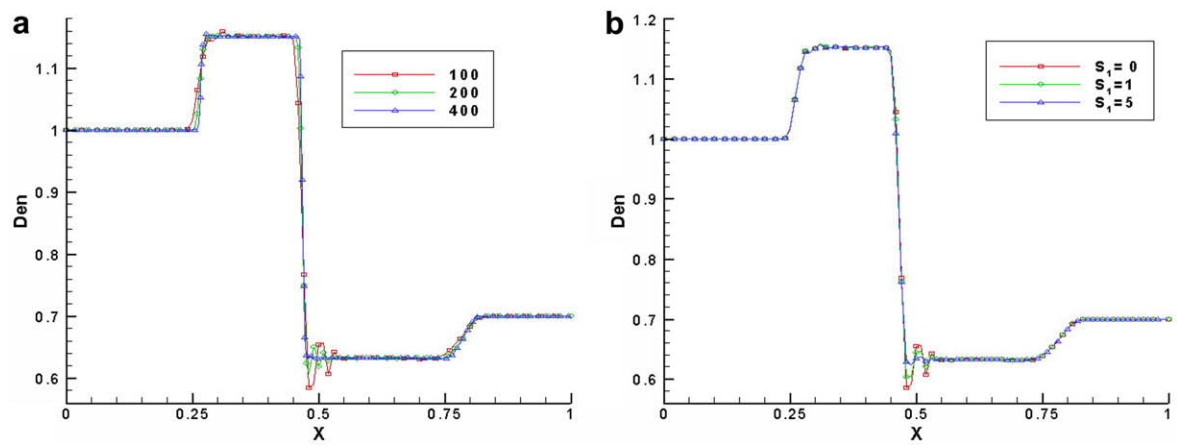

Fig. 6. Tests on large effective diameter $d = 100$, density profile: (a) grid refinement; (b) modified relaxation time.

Example 2 (*Effect of spatial reconstruction*). In this example, we test the accuracy of the reconstruction using van Leer slope limiter. Without using the slope limiter, i.e., using only constant state, we have first-order spatial accuracy. If we assume constant state of macroscopic variables, then $Df^{(0)} = 0$ in Eq. (30) due to no spatial gradients of those macroscopic variables and we are solving the Euler equation. We denote the scheme based on constant state as Eu_1.

The initial flow conditions are the same as in Example 1. The number of grids used is 100. The relaxation time is set to $\tau = 10^{-10}, 0.0001, 0.001$, and 0.01, respectively. The results for the Eu_1 and NS_2 schemes for different values of constant τ are shown in Fig. 3. In Figs. 3a and b, the relaxation times are small and the physical dissipation due to viscosity is also small and

sharper profiles can be obtained using the NS_2 method as compared to that obtained using Eu_1 method in which numerical dissipation is dominant. As the constant τ value is getting larger (from Figs. 3a–c), the profiles are getting smoother reflecting the fact that the corresponding viscosity (physical dissipation) is becoming larger. In Fig. 3c, the magnitude of the physical viscosity of NS_2 becomes comparable or larger than the numerical dissipation of Eu_1. The profile of NS_2 looks more smoother than that of Eu_1.

For the case of $\tau = 10^{-10}$ (Fig. 3d), we have $\tau \ll \Delta t$ and the physical viscosity is very small relative to numerical viscosity. The solution displays some oscillations which is due to the under-resolution of the flow structures. Usually, by refining the mesh, the amplitude of oscillation can be reduced.

Example 3 (*Tests on physical viscosity*). In this example, the second-order reconstruction based on van Leer slope limiter is used. We show the results of letting the initial distribution $f_0 = f^{(0)}$, which corresponding to the Euler solution, denoted as Eu_2 and $f_0 = f^{(0)} - \tau D f^{(0)}$, denoted as NS_2, respectively. The relaxation time is set to three different values, $\tau = 10^{-10}, 0.1, 0.0001$. In Fig. 4, the density profile for the two cases are shown. Here, the box symbol □ denotes the NS_2 solution. The results of symbol □ are exactly the same as the Example 2 with van Leer limiter. The triangle symbol △ denotes Eu_2 solution. We can find from Fig. 4 that the result of NS_2 is always more diffusive than that of Eu_2 in all three constant relaxation times. In the case of $\tau = 10^{-10}$, these two results overlaps. This shows that if the relaxation time is very small, then the physical viscosity will become very small also and there is no difference between the results using $f_0 = f^{(1)}$ and $f_0 = f^{(0)}$, as expected.

Example 4.1 (*Physical relaxation time*). This example uses the physical relaxation time defined in Eq. (60) which is a function of physical variables instead of constant value. The effective diameter of the quantum gas in each case is selected, respectively, as $d = 5, 10, 100$ in dimensionless units. The results are shown in Fig. 5. In the case of $d = 100$, one can find the resolution of the results is sharper but there is oscillation behind the shock. This is because the relaxation time of this quantum gas is too small and we have under-resolved the flow structures due to not fine enough grid size used and some oscillations

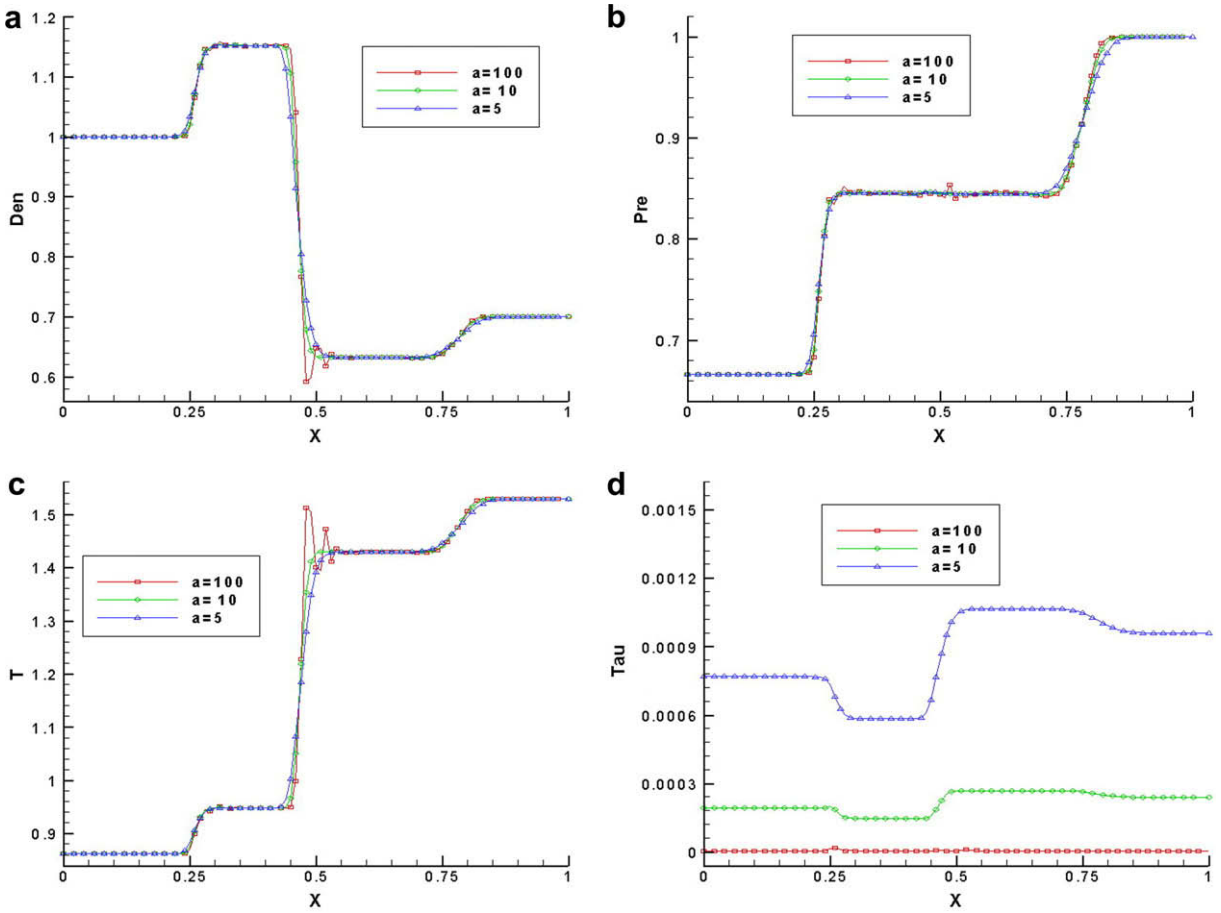

Fig. 7. Tests on different scattering length: (a) density; (b) pressure; (c) temperature; (d) relaxation time.

appear. In the $d = 10$ case, the solution is found to be more diffusive than that for the $d = 5$ case and in both cases the oscillations disappear. The order of relaxation time in each case is about 10^{-5} in the $d = 100$ case, and 10^{-3} in both $d = 5$ and $d = 10$ cases. The order of mean velocity and sound speed are about 10^{-1} and 1, respectively. The size of the grid cell is 0.01. So, the CFL time step Δt will be about 10^{-3}.

If we refine the grids, we can observe that the oscillations are greatly reduced. These results are shown in Fig. 6a for the $d = 100$ case. In Fig. 6a, the grid numbers are increased from 100 to 200 and 400. The oscillations behind the shock were reduced as expected. In Fig. 6b, we keep the number of grids to 100 but use the modified relaxation time devised by Xu, i.e., Eq. (62), $\tau_{\mathrm{mod}} = \tau_{\mathrm{phys}} + S_1 \Delta t |p_{\mathrm{L}} - p_{\mathrm{R}}| / |p_{\mathrm{L}} + p_{\mathrm{R}}|$, where p_{L} and p_{R} are quantum pressures constructed in the left and right

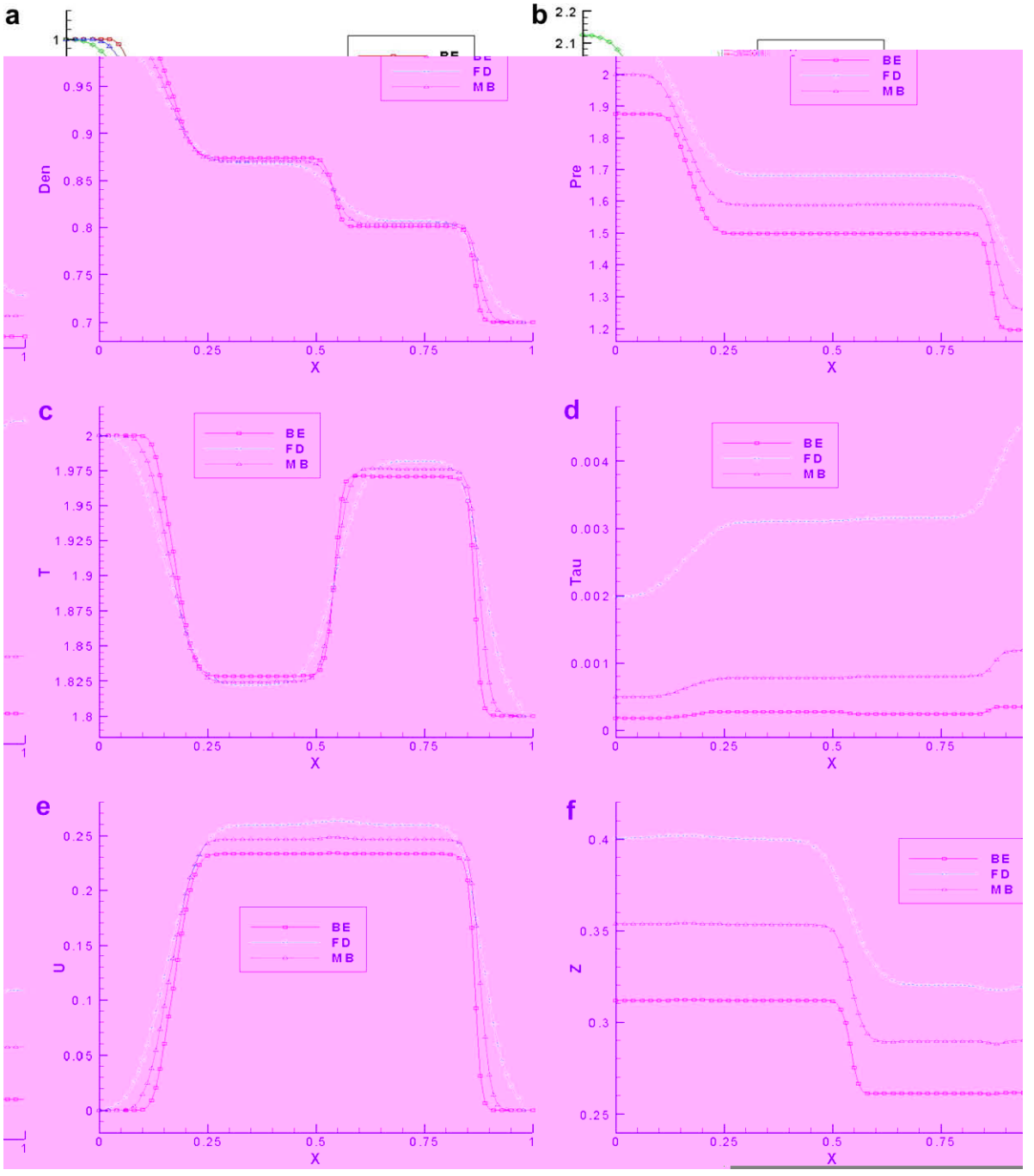

Fig. 8. The effect under different statistics: BE, Bose–Einstein; FD, Fermi–Dirac; MB, Maxwell–Boltzmann: (a) density; (b) pressure; (c) temperature; (d) relaxation time; (e) mean velocity; (f) fugacity.

sides of the cell interface, S_1 is a constant, and τ_{phys} is the physical relaxation time discussed above. When the modified relaxation time is used, we can find that the second term of τ_{mod} will be equal to zero if the flow is well resolved and the modified relaxation time will be equal to physical relaxation time. If the flow is not well resolved, this term introduces dissipations and the oscillations are reduced. Different values of S_1 are tested in Fig. 6b.Example 4.2 Scattering lengthThis example uses the physical relaxation time defined by Eq. (61) for a Boson gas which is a function of physical variables instead of constant value. This case considers different scattering length a to present different magnitudes of viscosity. The scattering length in some situations can be found in Nikuni and Griffin [16] for bosons. The scattering length of each case is selected as $a = 5, 10, 100$, separately and $S_1 = 1.0$ in every case. The results of different scattering length are shown in Fig. 7. For larger value of $a = 100$, the viscosity is small and hence the relaxation time is small (as can be seen from Fig. 7d), and the solution displays oscillations. For the cases of $a = 5$ and $a = 10$, the solutions are smooth and no oscillations are observed.

Example 5 (*Different statistics*). In this example, we compare the different behaviors of the three statistics, namely, Bose–Einstein, Fermi–Dirac, and Maxwell–Boltzmann statistics. We fix the initial number density and initial temperature in all three statistics. In the cases of quantum statistics, the physical relaxation times used are based on Eq. (60) with the effective diameter $d = 5$ and in the modified relaxation time, Eq. (62), we take $S_1 = 1$. In the case of Maxwell–Boltzmann statistics, the relaxation time used is

$$\tau_c = \frac{1}{4\sqrt{\pi} n d^2}(m/k_B T)^{1/2} + S_1 \Delta t |p_{L,cl} - p_{R,cl}|/|p_{L,cl} + p_{R,cl}|. \tag{63}$$

The initial conditions at the left and the right sides of the diaphragm in the shock tube are $(n_L, u_L, T_L) = (1.0, 0.0, 2.0)$ and $(n_R, u_R, T_R) = (0.7, 0.0, 1.8)$. The number of grids used is 100. The results are shown in Fig. 8, and we can clearly delineate the difference of three statistics. It is shown that under different statistics although the initial temperature, density, and effective diameters are the same, the pressure, internal energy, and the relaxation times are different. The FD result is the most diffusive one and the BE result is the least diffusive one among the three statistics and the MB result lies in between.

Next we consider the case that the temperatures on both sides of the diaphragm at initial time $t = 0$ are much higher. The initial conditions at the left and the right sides of the diaphragm are set as $(n_L, u_L, T_L) = (1.0, 0.0, 10.)$ and

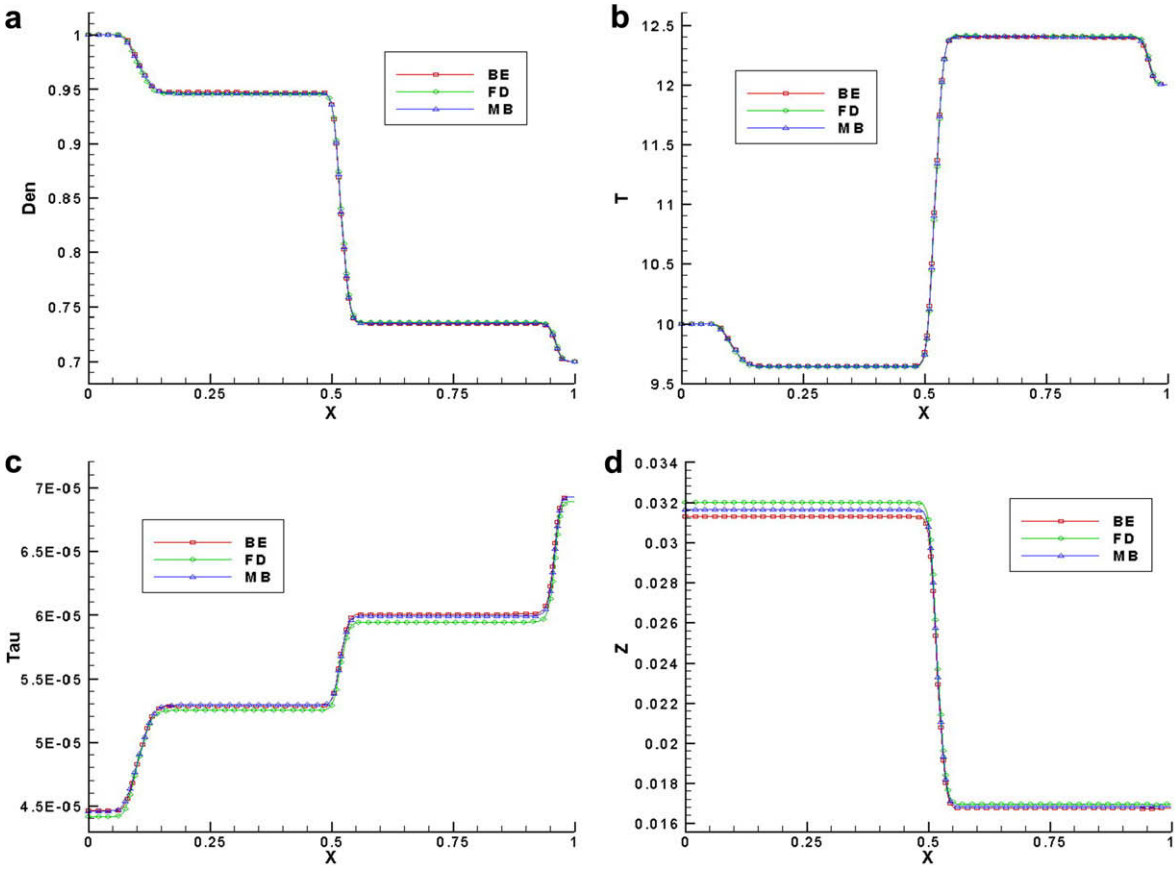

Fig. 9. The high-temperature limit under different statistics: BE, Bose–Einstein; FD, Fermi–Dirac; MB, Maxwell–Boltzmann: (a) density; (b) temperature; (c) relaxation time; (d) fugacity.

$(n_R, u_R, T_R) = (0.7, 0.0, 12.)$. Here, we still fix the initial number density and initial temperature but only increase the values of initial temperature on both sides, i.e., in the high-temperature limit. The purpose of choosing these conditions is to show that the classical limit of quantum statistics will recover the classical one under high temperature limit. The computation was done with 100 uniform grids and CFL = 0.5, and the results were output at time $t = 0.2$ and shown in Fig. 9. It is observed that the macroscopic properties of the three statistics are close to each other except for some small deviations. The present example confirms that in the high-temperature limit, the gas displays classical behaviors.

6. Concluding remarks

In this work, a class of gas-kinetic quantum BGK schemes for quantum hydrodynamic transport has been derived based on the semiclassical Boltzmann equation with relaxation time approximation. The present development is parallel to the classical counterpart of Xu's gas-kinetic BGK framework [23]. The present construction provides the quantum Navier–Stokes order solution. Due to the more complex form of the quantum equilibrium distribution, some new features of the QBGK schemes are delineated. A second-order reconstruction procedure using van Leer's limiter was adopted to achieve second-order accuracy in time and space. The resulting quantum gas-kinetic scheme was applied to simulate one-dimensional quantum gas flow in a shock tube to illustrate the method. Several formulas for the relaxation time are employed and the present schemes have been tested for wide range of values of relaxation time and thus wide values of viscosity. The hydrodynamic limit of both Euler and Navier–Stokes solutions are shown. Both Bose–Einstein and Fermi–Dirac gas transport can be considered. Several numerical validations are shown in this work. The effects of quantum degeneracy in different statistics are also depicted in the present results. One can find that not only the statistics difference but also the dynamics difference between Maxwell–Boltzmann, Bose–Einstein, and Fermi–Dirac distributions in the simulation. New formulations for half-ranged moment integrations of the quantum equilibrium distribution function used in the present work are included in the Appendix. The moment integration can recover the classical formulation once the incomplete gamma functions are replaced by error function. The present formulation and derivation are rather general and the extension to multi-dimensional problems can be done directly and will be reported elsewhere.

Acknowledgment

This work is done under the auspices of National Science Council, Taiwan through Grants NSC 95-2212E-002-342-MY3.

Appendix A

We introduce some notations to make the presentation more concise. First, the moments of the distribution function are denoted as

$$\langle f^{(0)}\rangle_{pq} = \int_{-\infty}^{\infty} c^p \xi^{2q} f^{(0)}\,\mathrm{d}c\,\mathrm{d}\Xi', \quad \langle f'^{(0)}\rangle_{pq} = \int_{-\infty}^{\infty} c^p \xi^{2q} f'^{(0)}\,\mathrm{d}c\,\mathrm{d}\Xi', \tag{A.1}$$

$$\langle f^{(0)}\rangle_{pq}^{<0} = \int_{-\infty}^{0} c^p \xi^{2q} f^{(0)}\,\mathrm{d}c\,\mathrm{d}\Xi', \quad \langle f'^{(0)}\rangle_{pq}^{>0} = \int_{0}^{\infty} c^p \xi^{2q} f'^{(0)}\,\mathrm{d}c\,\mathrm{d}\Xi', \tag{A.2}$$

$$\langle f^{(0)}\rangle_{pq}^{>0} = \int_{0}^{\infty} c^p \xi^{2q} f^{(0)}\,\mathrm{d}c\,\mathrm{d}\Xi', \quad \langle f'^{(0)}\rangle_{pq}^{<0} = \int_{-\infty}^{0} c^p \xi^{2q} f'^{(0)}\,\mathrm{d}c\,\mathrm{d}\Xi'. \tag{A.3}$$

The above moments are integrated with respect to the molecular velocity c. We need to define the moments which are integrated with respect to peculiar velocity c' and give the general formulation

$$\int_{-\infty}^{\infty}\int_{-\infty}^{\infty}\int_{0}^{\infty} c_x'^{\alpha} c_y'^{\beta} c_z'^{\gamma} f^{(0)} \frac{\mathrm{d}^3 p}{h^3} = D_{\alpha\beta\gamma} Q_{(\alpha+\beta+\gamma+3)/2}(z), \tag{A.4}$$

$$\int_{-\infty}^{\infty}\int_{-\infty}^{\infty}\int_{0}^{\infty} c_x'^{\alpha} c_y'^{\beta} c_z'^{\gamma} f'^{(0)} \frac{\mathrm{d}^3 p}{h^3} = D_{\alpha\beta\gamma} Q_{(\alpha+\beta+\gamma+1)/2}(z), \tag{A.5}$$

$$\int_{-\infty}^{\infty}\int_{-\infty}^{\infty}\int_{0}^{U} c_x'^{\alpha} c_y'^{\beta} c_z'^{\gamma} f^{(0)} \frac{\mathrm{d}^3 p}{h^3} = \frac{D_{\alpha\beta\gamma}}{\Gamma\left(\frac{\alpha+1}{2}\right)} \Theta_{(\alpha+\beta+\gamma+3)/2}(z, \lambda U^2), \tag{A.6}$$

$$\int_{-\infty}^{\infty}\int_{-\infty}^{\infty}\int_{0}^{U} c_x'^{\alpha} c_y'^{\beta} c_z'^{\gamma} f'^{(0)} \frac{\mathrm{d}^3 p}{h^3} = \frac{D_{\alpha\beta\gamma}}{\Gamma\left(\frac{\alpha+1}{2}\right)} \Theta_{(\alpha+\beta+\gamma+1)/2}(z, \lambda U^2), \tag{A.7}$$

$$D_{\alpha\beta\gamma} = \frac{\Gamma\left(\frac{\alpha+1}{2}\right)\Gamma\left(\frac{\beta+1}{2}\right)\Gamma\left(\frac{\gamma+1}{2}\right)}{2\lambda^{(\alpha+\beta+\gamma)/2}\Lambda^3\pi^{3/2}} \left(\frac{(-1)^{\beta}+1}{2}\right)\left(\frac{(-1)^{\gamma}+1}{2}\right). \tag{A.8}$$

The functions $Q_n(z)$ and $\Theta_n(z,h)$ used above are the BE (FD) function and incomplete BE (FD) function, respectively,

$$\Theta_n(z,h) \equiv \int_0^h \frac{x^{n-1}}{z^{-1}\mathrm{e}^x+\theta}\,\mathrm{d}x = \sum_{l=1}^{\infty}(-\theta)^{l-1}\frac{z^l}{l^n}\Gamma(n+1,lh), \tag{A.9}$$

$$z^{-1}\int_0^h \frac{x^n\mathrm{e}^x}{(z^{-1}\mathrm{e}^x+\theta)^2}\,\mathrm{d}x = \sum_{l=1}^{\infty}(-\theta)^{l-1}\frac{z^l}{l^n}\Gamma(n+1,lh), \tag{A.10}$$

$$\frac{z^{-1}}{\Gamma(n+1)}\int_0^\infty \frac{x^n\mathrm{e}^x}{(z^{-1}\mathrm{e}^x+\theta)^2}\,\mathrm{d}x = \sum_{l=1}^{\infty}(-\theta)^{l-1}\frac{z^l}{l^n}, \tag{A.11}$$

$$\Gamma(a,x) = \int_0^x t^{a-1}\mathrm{e}^{-t}\,\mathrm{d}t. \tag{A.12}$$

Finally, we can use these two notations to all situation of integration.

$$I^{>0}_{(f,m)} = \int_{c_x>0} c_x^m f\phi\,\mathrm{d}\Xi, \quad II^{\bar{A}}_{(f',m)} = \int c_x^m \bar{A} f'\phi\,\mathrm{d}\Xi. \tag{A.13}$$

The superscripts $>0, <0$ of I and II represent the limited range of the particle velocity and no limitation is imposed if not declared. In II the remaining superscript means the corresponding coefficient matrix ($a_l, \bar{a}_r, \ldots$). The subscript on the left is the kind of distribution function (f_l, f_r, f_0), and m on the right is the power (or order) of c_x. Here are two examples of these two notations

$$I^{>0}_{(g_l,1)} = \int c_x H(c_x) g_l \phi\,\mathrm{d}\Xi = \begin{bmatrix} \langle g_l\rangle^{>0}_{10} \\ \langle g_l\rangle^{>0}_{20} \\ m(\langle g_l\rangle^{>0}_{30} + \langle g_l\rangle^{>0}_{21})/2 \end{bmatrix}, \tag{A.14}$$

$$II^{(\bar{a}_r,<0)}_{(f_r'^{(0)},2)} = \int c_x^2 \bar{a}^r \overline{H}(c_x) f_r'^{(0)}\phi\,\mathrm{d}\Xi = \begin{bmatrix} \bar{a}_{r1}\langle f_r'^{(0)}\rangle^{<0}_{20} + \bar{a}_{r2}\langle f_r'^{(0)}\rangle^{<0}_{30} + \bar{a}_{r3}m(\langle f_r'^{(0)}\rangle^{<0}_{40} + \langle f_r'^{(0)}\rangle^{<0}_{22})/2 \\ \bar{a}_{r1}\langle f_r'^{(0)}\rangle^{<0}_{30} + \bar{a}_{r2}\langle f_r'^{(0)}\rangle^{<0}_{40} + \bar{a}_{r3}m(\langle f_r'^{(0)}\rangle^{<0}_{50} + \langle f_r'^{(0)}\rangle^{<0}_{32})/2 \\ \bar{a}_{r1}m(\langle f_r'^{(0)}\rangle^{<0}_{40} + \langle f_r'^{(0)}\rangle^{<0}_{21})/2 + \bar{a}_{r2}m(\langle f_r'^{(0)}\rangle^{<0}_{50} + \langle f_r'^{(0)}\rangle^{<0}_{31})/2 \\ +\bar{a}_{r3}m^2(\langle f_r'^{(0)}\rangle^{<0}_{60} + 2\langle f_r'^{(0)}\rangle^{<0}_{41} + \langle f_r'^{(0)}\rangle^{<0}_{22})/4 \end{bmatrix}. \tag{A.15}$$

With these notations, the time average flux can be expressed as

$$\begin{aligned} F_0 &= I_{(g_0,1)} + \frac{\triangle t}{2} II^{\bar{A}}_{(g_0',1)}, \\ F_1 &= \gamma_1 I_{(g_0,1)}, \\ F_2 &= \gamma_2 (II^{(\bar{a}^l,>0)}_{(g_l',2)} + II^{(\bar{a}^r,<0)}_{(g_r',2)}), \\ F_3 &= \gamma_3 (I^{>0}_{(g_l,1)} + I^{<0}_{(g_r,1)}), \\ F_4 &= \gamma_4 (II^{(a^l,>0)}_{(g_l',2)} + II^{(a^r,<0)}_{(g_r',2)}), \\ F_5 &= \gamma_5 (II^{(A^l,>0)}_{(g_l',1)} + II^{(A^r,<0)}_{(g_r',1)}), \\ F_6 &= \gamma_6 II^{\bar{A}}_{(g_0',1)}. \end{aligned} \tag{A.16}$$

Apply the compatibility condition to solve the coefficient $\bar{A}$, one has

$$\begin{aligned} -\gamma_6 \int \phi_\alpha \bar{A} g_0'\,\mathrm{d}\Xi = \int \{&\gamma_1 g_0 + \gamma_2 c(\bar{a}^l H(c_x) + \bar{a}^r \overline{H}(c_x)) g_0' \\ &+ \gamma_3 [H(c_x) f_l'^{(0)} + \overline{H}(c_x) f_r'^{(0)}] + \gamma_4 c[a_l H(c_x) f_l'^{(0)} + a_r \overline{H}(c_x) f_r'^{(0)}] \\ &+ \gamma_5 [A_l H(c_x) f_l'^{(0)} + A_r \overline{H}(c_x) f_r'^{(0)}]\}\phi\,\mathrm{d}\Xi, \end{aligned} \tag{A.17}$$

$$\begin{aligned} \gamma_1 &= (\tau/\Delta t)(-1+\mathrm{e}^{-\Delta t/\tau}), \\ \gamma_2 &= (\tau/\Delta t)(-\Delta t + 2\tau - \mathrm{e}^{-\Delta t/\tau}(\Delta t + 2\tau)), \\ \gamma_3 &= (\tau/\Delta t)(1-\mathrm{e}^{-\Delta t/\tau}), \\ \gamma_4 &= (\tau/\Delta t)(-2\tau + \mathrm{e}^{-\Delta t/\tau}(\Delta t + 2\tau)), \\ \gamma_5 &= (\tau/\Delta t)\tau(\mathrm{e}^{-\Delta t/\tau} - 1), \\ \gamma_6 &= (\tau/\Delta t)(-\Delta t + \tau - \tau\mathrm{e}^{-\Delta t/\tau}) \end{aligned} \tag{A.18}$$

and

$$-\gamma_6 II^{\bar{A}}_{g_0,0} = \gamma_1 I^{\bar{A}}_{(g_0,0)} + \gamma_2 (II^{(\bar{a}^l,>)}_{(g_0',1)} + II^{(\bar{a}^r,<)}_{(g_0',1)}) + \gamma_3 (I^{>}_{(f_l'^{(0)},0)} + I^{<}_{(f_r'^{(0)},0)}) + \gamma_4 (II^{(a^l,>)}_{(f_l'^{(0)},1)} + II^{(a^r,<)}_{(f_r'^{(0)},1)}) + \gamma_5 (II^{(A^l,>)}_{(f_l'^{(0)},0)} + II^{(A^r,<)}_{(f_r'^{(0)},0)}). \tag{A.19}$$

References

[1] J. Beyer, Effect of a convex boundary on a rarefied classical or quantum gas: flow past a stationary boundary and the effect of an oscillating boundary on the gas, Phys. Rev. B 33 (1986) 511–525.
[2] P.L. Bhatnagar, E.P. Gross, M. Krook, A model for collision processes in gases, I. Small amplitude processes in charged and neutral one-component system, Phys. Rev. 94 (3) (1954) 511–525.
[3] G.A. Bird, Molecular Gas Dynamics and the Direct Simulation of Gas Flow, second ed., Oxford University Press, Oxford, 1994.
[4] S. Chapman, T.G. Cowling, The Mathematical Theory of Non-Uniform Gases, Cambridge University Press, 1970.
[5] G. Chen, Nanoscale Energy Transport and Conversion, Oxford University Press, 2005.
[6] S.Y. Chou, D. Baganoff, Kinetic flux-vector splitting for the Navier–Stokes equations, J. Comput. Phys. 130 (1997) 217–230.
[7] P. Degond, C. Ringhofer, Quantum moment hydrodynamics and the entropy principle, J. Stat. Phys. 112 (2003) 587–628.
[8] A.L. Garcia, W. Wagner, Direct simulation Monte Carlo method for the Uehling–Uhlenbeck–Boltzmann equation, Phys. Rev. E 68 (2003) 056703.
[9] C.L. Gardner, The quantum hydrodynamic model for semiconductor devices, SIAM J. Appl. Math. 54 (1994) 409–427.
[10] C.L. Gardner, C. Ringhofer, The Chapman–Enskog expansion and the quantum hydrodynamic model for semiconductor devices, VLSI Des. 10 (2000) 415–435.
[11] A. Griffin, W.C. Wu, S. Stringari, Hydrodynamic modes in a trapped Bose gas above the Bose–Einstein transition, Phys. Rev. Lett. 78 (1997) 1838.
[12] T.Y. Hsieh, J.Y. Yang, Y.H. Shi, Kinetic flux vector splitting schemes for ideal quantum gas dynamics, SIAM J. Sci. Comput. 29 (2007) 221–244.
[13] K. Huang, Statistical Mechanics, second ed., Wiley, New York, 1987.
[14] L.P. Kadanoff, G. Baym, Quantum Statistical Mechanics, Benjamin, New York, 1962 (Chapter 6).
[15] M. Lundstrom, Fundamentals of Carrier Transport, second ed., Cambridge University Press, Cambridge, 2000.
[16] T. Nikuni, A. Griffin, Hydrodynamic damping in trapped Bose gases, J. Low Temp. Phys. 111 (1998) 793–814.
[17] T. Ohwada, The kinetic scheme for the full-Burnett equations, J. Comput. Phys. 201 (2004) 315–332.
[18] P.F. Santos, J. Léonard, J. Wang, C.J. Barrelet, F. Perales, E. Rasel, Bose–Einstein condensation of metastable helium, Phys. Rev. Lett. 86 (2001) 3459–3462.
[19] E.A. Uehling, G.E. Uhlenbeck, Transport phenomena in Einstein–Bose and Fermi–Dirac gases. I, Phys. Rev. 43 (1933) 552.
[20] E. Wigner, On the quantum correction for thermodynamic equilibrium, Phys. Rev. 40 (1932) 749–759.
[21] K. Xu, K.H. Prendergast, Numerical Navier–Stokes solutions from gas-kinetic theory, J. Comput. Phys. 114 (1994) 9.
[22] K. Xu, Gas-kinetic scheme for unsteady compressible flow simulations, in: VKI for Fluid Dynamics Lecture Series, 1998–2003, 1998.
[23] K. Xu, A gas-kinetic BGK scheme for the Navier–Stokes equations and its connection with artificial dissipation and Godunov method, from gas-kinetic theory, J. Comput. Phys. 171 (2001) 289–335.
[24] K. Xu, M. Mao, L. Tang, A multidimensional gas-kinetic BGK scheme for hypersonic viscous flow, J. Comput. Phys. 203 (2005) 405–421.
[25] J.Y. Yang, J.C. Huang, Rarefied flow computations using nonlinear model Boltzmann equations, J. Comput. Phys. 120 (1995) 323–339.
[26] J.Y. Yang, Y.H. Shi, A kinetic beam scheme for the ideal quantum gas dynamics, Proc. Roy. Soc. Lond. A 462 (2006) 1553.